Available online at www.jourcc.com

Journal homepage: www.JOURCC.com

Journal of Composites and Compounds

Synthesis and mechanical properties of Bi_2O_3-$Al_4Bi_2O_9$ nanopowders

Shayan Askari [a]*, ***Majid Ghashang*** [a], ***Ghazal Sohrabi*** [a]

[a] *Department of Chemistry, Najafabad Branch, Islamic Azad University (IAU), Isfahan, Iran*

A B S T R A C T

As a result of great surface area and a great number of energetic sites, ceramic nanocomposites are being considered as good adsorbents and catalysts. Al_2O_3 nanoparticles are widely used in high-tech applications owing to their excellent properties. Besides, Bi-based oxides have been the center of attention for applications such as remediation of hazardous wastes and wastewater photochemical degradation of organic contaminants and remediation of hazardous wastes. In this research, the synthesis of Bi_2O_3-$Al_4Bi_2O_9$ nanocomposite and its mechanical properties as a novel composition were investigated. The results showed that the prepared Bi_2O_3-$Al_4Bi_2O_9$ sample exhibited the $Al_4Bi_2O_9$ crystalline peaks. Additionally, the prepared nanocomposite showed no impurities. The mechanical properties of the Bi_2O_3-$Al_4Bi_2O_9$ sample were improved in comparison with Al_2O_3, Bi_2O_3, and Bi_2O_3- Al_2O_3, which offer it as a promising alternative to Bi_2O_3-Al_2O_3 composite ceramic.

Peer review under responsibility of JCC Research Group

A R T I C L E I N F O R M A T I O N

Article history:
Received 06 October 2020
Received in revised form 10 November 2020
Accepted 19 December 2020

Keywords:
Nanocomposite
Catalyst
Al_2O_3
Bi_2O_3-$Al_4Bi_2O_9$
Novel composition

1. Introduction

Due to significant advances in the production of nanostructured materials with new properties, many researchers have focused on the engineering of multi-functional macroscopic materials by structure design at the nanometer scale. One of the fast-growing areas of composites research is the development of nanocomposites [1, 2].

Novel material properties can be achieved by decreasing the particle size to the nanometer scale [3]. In addition to the properties of the matrix and reinforcement, the properties of nanocomposite depend on the morphology and interfacial characteristics of the constituents [4, 5]. The surface area to volume ratio of reinforcements is a morphological property determining the relationship between the structure and property of nanocomposites [3].

Nanocrystalline ceramics have the potential to be used as catalyst supports [6, 7] and adsorbents [8-11] owing to possessing a large surface area and a high number of energetic sites for the interaction with contaminants [12, 13]. Due to the excellent properties of Al_2O_3 nanoparticles, they have found ways to the ceramic industry and high-tech applications [14]. Crystal phases of Al_2O_3 include η, δ, θ, γ, and α-Al_2O_3, and among all these phases, the strongest absorption belongs to α and γ due to possessing the highest surface area for the majority of photocatalytic reactions [15-18].

Owing to properties such as good environmental compatibility, dielectric permittivity, low toxicity, high retractile indicator, and convenient band gap energy about 2.8 eV, Bi-based oxides, especially Bi_2O_3, have been widely studied. These oxides are good candidates for different green applications including remediation of hazardous waste substances and photochemical (visible light) degradation of organic contaminants in wastewater [18-25] Bi_2O_3 is used in some industries including optical coatings, gas sensors, optoelectronics, and solid oxide fuel cells [26, 27]. Trivedi et al. [28] studied the thermal, physical, and atomic properties of Bi_2O_3 treated by biofield energy [29]. According to the results, the physical and atomic characteristics of Bi_2O_3 changed by biofield energy treatment, which makes it more useful to be used in solid oxide fuel cells [30].

Dehkordi et al. [31] used Transient Liquid Phase (TLP) route by Bi_2O_3 reinforcement to join alumina to alumina. Bi_2O_3 was used because of its low melting point [32]. A thin interlayer of Bi_2O_3 was placed between the ceramic bodies [33]. The results showed the interfacial compound growth between Bi_2O_3 and Al_2O_3 at 880 °C upon the TLP process [34]. Higher mechanical properties of the interfaces were observed for longer joining times. Neiman et al. [35] studied differences between the interaction of microsized Al_2O_3 or nanosized Al_2O_3 with microsized Bi_2O_3 [36]. Nano-Al_2O_3 showed higher reactivity and stronger adhesion to micro-Bi_2O_3 leading to the encapsulation of micro-Bi_2O_3 in a shell composed of Al_2O_3 and interaction products [37]. Above 400 °C, the presence of $BiAlO_3$, $Al_2Bi_{24}O_{39}$, and $Al_4Bi_2O_9$ phases was confirmed, and at higher temperatures, the main complex intermediate was $Al_4Bi_2O_9$. At 730 °C, phase transfer from α-Bi_2O_3 to δ-Bi_2O_3 was achieved. By further increase in the temperature to 780 °C, the solid phase was decomposed in interaction products, and the δ-Bi_2O_3 phase was separated. The grains of δ-Bi_2O_3 [38] with high conductivity formed a connected charge percolation resulting in a 2.5-fold conductivity increase between 770 °C to 800 °C.

Different methods are employed for the production of metal oxide nanoparticles including electrodeposition, precipitation, sol-gel, hydrothermal, and combustion methods [39, 40]. A common synthesis method is the sol-gel route. Homogeneity and the production of high purity

* *Corresponding author: Shayan Askari; E-mail: shayan_askari@ymail.com*
DOR: 20.1001.1.26765837.2020.2.5.2.6
https://doi.org/10.29252/jcc.2.4.2

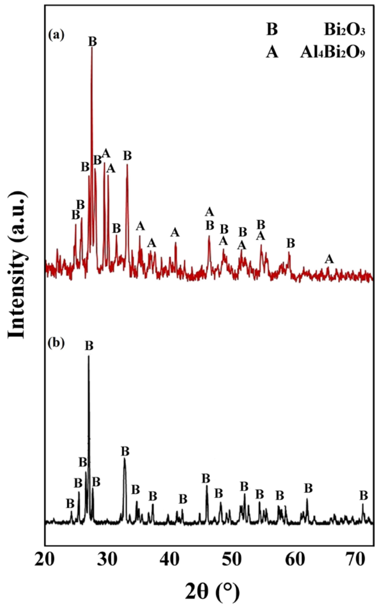

Fig. 1. XRD patterns of the (a) Bi_2O_3-$Al_4Bi_2O_9$ and (b) Bi_2O_3 nanopowders.

materials are some advantages of the sol-gel method [41, 42]. In this study, Bi_2O_3-$Al_4Bi_2O_9$ nanocomposite was synthesized using the sol-gel method and its mechanical properties were evaluated. Based on previous studies regarding the phases formed in Bi_2O_3 and Al_2O_3 nanocomposites, this new nanocomposite is expected to have improved mechanical properties and can be utilized as novel and efficient materials for various applications.

2. Materials and methods

2.1. Materials

All reagents and chemicals i.e. Bismuth (III) nitrate ($Bi(NO_3)_3$, Aluminum nitrate nonahydrate ($Al(NO_3)_3$) and Ethanolamine (2-Aminoethanol) C_2H_7NO in this research were obtained from Merck (Darmstadt, Germany) without further purification. All Glass containers underwent alkali washing and rinsing before application.

Synthesis procedure

To prepare the samples, 300 mmol of 2-aminoethanol was added to 50 ml of water. Then, the solution was added dropwise to a solution containing aluminum nitrate (40 mmol) and $Bi(NO_3)_3$ (40 mmol) in distilled water (200 ml) while the solution was stirred during mixing. Stirring continued for another 60 min. Finally, the precipitates were filtered, washed, and heat-treated at 600 °C for 3 h.

2.2. Characterization

The tensile properties of the nanocomposites were evaluated as per D3039-ASTM at room temperature at a crosshead speed of 5 mm/min using an Instron 6025 device. The samples were prepared by sintering (600 °C for 3 h) with dimensions of 150 × 25 × 3 mm. A three-point bending tester (Instron 6025) was used to measure the bending strength of the nanocomposites. The test was performed according to D790-ASTM at a crosshead speed of 2 mm/ min at room temperature. The length, width, and thickness of the samples were 90 mm, 10 mm, and 3 mm, respectively. A Zwick pendulum impact tester was used to study the impact strength of the samples. The results are the average of five repetitions.

The Vickers hardness of the samples was measured at ambient temperature using Instron, Wilson-Wolpert Tukon 2100B. The applied load and loading time was 10 N and 10 s, respectively. The samples were polished prior to the measurement and the measurement was repeated three times for each sample. The structure of the powders was studied using X-ray diffraction analysis (XRD) (Philips X' Pert, The Netherlands) operating at 30 mA and 40 kV. Cu-Kα radiation with λ = 15.405 nm was used, and the step size was 0.02˚. X'Pert HighScore software was utilized to identify the crystalline phases of the powder [43]. The gold-coated fracture surface of the samples was studied by the scanning electron microscopy **(**SEM) analysis (Hitachi S-3400N, Japan). The operating voltage of the microscope was 15 kV [44, 45].

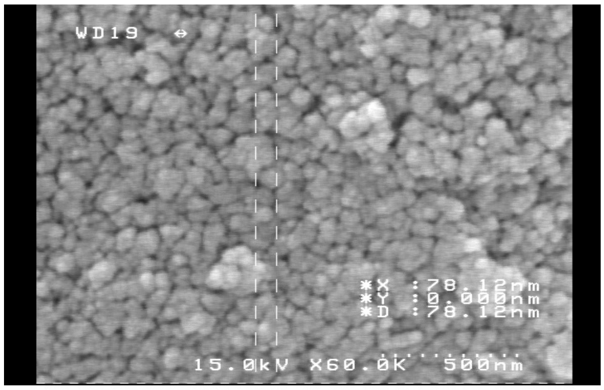

Fig. 2. SEM micrographs of the Bi_2O_3-$Al_4Bi_2O_9$ nanopowder.

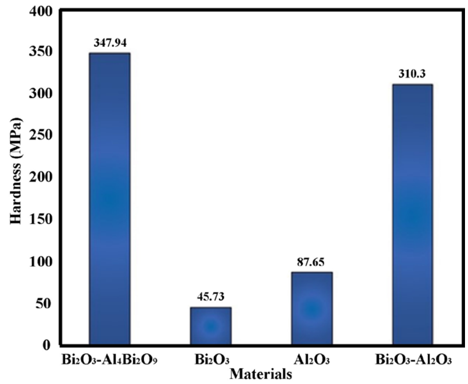

Fig. 3. Vickers hardness of the Bi_2O_3, Al_2O_3, Bi_2O_3-Al_2O_3, and Bi_2O_3-$Al_4Bi_2O_9$ samples.

3. Results and discussion

3.1. Microstructural analysis

To identify the crystal structure and parameters, the quantitative and non-destructive method of XRD is widely used. The XRD diffraction pattern of the prepared powder is illustrated in Fig.1. The peaks appeared at 2θ of 24.79°, 25.85°, 27.13°, 27.66°, 28.09°, 31.45°, 33.20°, and 46.51° are related to the Bi_2O_3 phase and the peaks at 15.83°, 29.64°, 30.21°, 35.21°, 41.10°, 48.82, 52.01, 54.91, and 59.35° represent the presence of $Al_4Bi_2O_9$. The $Al_4Bi_2O_9$ and Bi_2O_3 phases have monoclinic and orthorhombic crystal structures, respectively. Additionally, no impurities were detected in the powder composition. The average crystal sizes of the powder estimated from the Debye-Scherrer equation was obtained to be around 24 nm. The microstructure of the Bi_2O_3-$Al_4Bi_2O_9$ nanopowder is illustrated in Fig. 2. As seen, the particle size of the nanopowder is in the range of 30-60 nm.

3.2. Mechanical properties

The results of Vickers hardness for Al_2O_3, Bi_2O_3, Bi_2O_3-Al_2O_3, and Bi_2O_3-$Al_4Bi_2O_9$ are represented in Fig. 3. According to the results, the Bi_2O_3-$Al_4Bi_2O_9$ sample showed the highest hardness compared to other

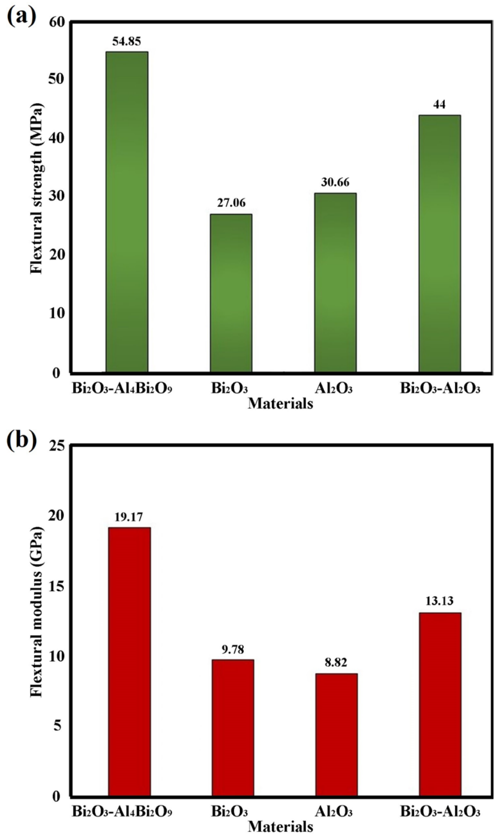

Fig. 4. (a) Flexural strength and (b) flexural modulus of the Bi_2O_3, Al_2O_3, Bi_2O_3-Al_2O_3 and Bi_2O_3-$Al_4Bi_2O_9$ samples

samples, revealing that the Bi_2O_3-$Al_4Bi_2O_9$ composite can be considered as a good alternative to the Al_2O_3-Bi_2O_3 composite. The Vickers hardness data indicated that Bi-O chemical bonds in Bi_2O_3-$Al_4Bi_2O_9$ composite are considerably strong. The Bi_2O_3-$Al_4Bi_2O_9$ samples exhibited 260.29, 302.21, and 37.64 MPa enhancement in Vickers hardness compared to Al_2O_3, Bi_2O_3, and Bi_2O_3-Al_2O_3, respectively. The increase in hardness in the composite indicates a good bond between the Bi_2O_3 and Al_2O_3.

The bending test was carried out to measure the flexural modulus and flexural strength of the samples. The flexural modulus and flexural strength of Al_2O_3, Bi_2O_3, Bi_2O_3-Al_2O_3, and Bi_2O_3-$Al_4Bi_2O_9$ samples are observed in Fig. 4. The results show that the highest value of bending strength is associated with Bi_2O_3-$Al_4Bi_2O_9$. Significant increase in flexural modulus and flexural strength of Bi_2O_3-$Al_4Bi_2O_9$ sample exhibited in Fig. 4. When we use Bi_2O_3 its impact on its mechanical properties such as flexural modulus and flexural strength can be seen. The good effect of Bi_2O_3-$Al_4Bi_2O_9$ can be attributed to the proper relationship created between Al_2O_3 and Bi_2O_3.

Failure toughness of the samples is obtained from the impact test. As shown in Fig.5, The fracture toughness of the Al_2O_3, Bi_2O_3, Bi_2O_3-Al_2O_3, and Bi_2O_3-$Al_4Bi_2O_9$ samples are 0.5, 0.6, 0.8, and 1.8, respectively. The Bi_2O_3-$Al_4Bi_2O_9$ samples showed the highest fracture toughness compared to other samples and Bi_2O_3 show the lowest fracture toughness. The most important reason that can be the cause of this result is the formation of agglomerates and agglomerates at Bi_2O_3, where failure occurs earlier than expected.

4. Conclusions

In this research, Bi_2O_3-$Al_4Bi_2O_9$ nanocomposite was synthesized via the sol-gel method. The formation of the $Al_4Bi_2O_9$ was confirmed by the XRD analysis without any impurities in the composite structure. The

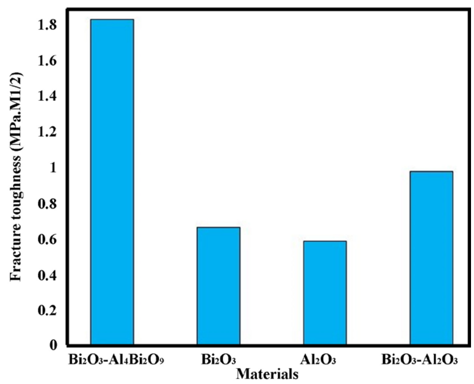

Fig. 4. Fracture toughness of the Bi_2O_3, Al_2O_3, Bi_2O_3-Al_2O_3, and Bi_2O_3-$Al_4Bi_2O_9$ samples

mechanical properties of the Al_2O_3, Bi_2O_3, Bi_2O_3-Al_2O_3, and Bi_2O_3-$Al_4Bi_2O_9$ samples were evaluated and the results showed that Vickers hardness, bending strength, and failure toughness of Bi_2O_3-$Al_4Bi_2O_9$ was the highest amount among other samples. Therefore, this ceramic composite can be a good alternative to the Bi_2O_3-Al_2O_3 composite.

Acknowledgments

The authors would like to acknowledge the Islamic Azad University (IAU) for the financial support towards this research.

Conflict of interest

The authors declare that there is no conflict of interest.

REFERENCES

[1] L. Bazli, A. Khavandi, M.A. Boutorabi, M. Karrabi, Morphology and viscoelastic behavior of silicone rubber/EPDM/Cloisite 15A nanocomposites based on Maxwell model, Iranian Polymer Journal 25(11) (2016) 907-918.

[2] L. Bazli, A. Khavandi, M.A. Boutorabi, M. Karrabi, Correlation between viscoelastic behavior and morphology of nanocomposites based on SR/EPDM blends compatibilized by maleic anhydride, Polymer 113 (2017) 156-166.

[3] E. Thostenson, C. Li, T. Chou, Nanocomposites in context, Composites Science and Technology 65(3-4) (2005) 491-516.

[4] F. Hussain, M. Hojjati, M. Okamoto, R.E. Gorga, Review article: Polymer-matrix Nanocomposites, Processing, Manufacturing, and Application: An Overview, Journal of Composite Materials 40(17) (2006) 1511-1575.

[5] L. Bazli, M.H. Bagherian, M. Karrabi, F. Abbassi-Sourki, H. Azizi, Effect of starch ratio and compatibilization on the viscoelastic behavior of POE/starch blends, Journal of Applied Polymer Science 137(29) (2020) 48877.

[6] J.R. Gaudet, A. de la Riva, E.J. Peterson, T. Bolin, A.K. Datye, Improved Low-Temperature CO Oxidation Performance of Pd Supported on La-Stabilized Alumina, ACS Catalysis 3(5) (2013) 846-855.

[7] H. Purón, J.L. Pinilla, C. Berrueco, J.A. Montoya de la Fuente, M. Millán, Hydrocracking of Maya Vacuum Residue with NiMo Catalysts Supported on Mesoporous Alumina and Silica–Alumina, Energy & Fuels 27(7) (2013) 3952-3960.

[8] M.M. Ibrahim, Cr_2O_3/Al_2O_3 as adsorbent: Physicochemical properties and adsorption behaviors towards removal of Congo red dye from water, Journal of Environmental Chemical Engineering 7(1) (2019) 102848.

[9] L.M. Camacho, A. Torres, D. Saha, S. Deng, Adsorption equilibrium and kinetics of fluoride on sol–gel-derived activated alumina adsorbents, Journal of Colloid and Interface Science 349(1) (2010) 307-313.

[10] J. Li, L. Xu, P. Sun, P. Zhai, X. Chen, H. Zhang, Z. Zhang, W. Zhu, Novel application of red mud: Facile hydrothermal-thermal conversion synthesis of hierarchical porous AlOOH and Al_2O_3 microspheres as adsorbents for dye removal, Chemical Engineering Journal 321 (2017) 622-634.

[11] K. Yang, Y. Li, Z. Zhao, Z. Tian, Y. Lai, Amorphous porous layered-Al_2O_3 derived from AlFu MOFs as an adsorbent for removing fluorine ions in industrial ZnSO4 solution, Chemical Engineering Research and Design 153 (2020) 562-571.

[12] A. Khaleel, P.N. Kapoor, K.J. Klabunde, Nanocrystalline metal oxides as new adsorbents for air purification, Nanostructured Materials 11(4) (1999) 459-468.

[13] K. Hristovski, A. Baumgardner, P. Westerhoff, Selecting metal oxide nanomaterials for arsenic removal in fixed bed columns: From nanopowders to aggregated nanoparticle media, Journal of Hazardous Materials 147(1) (2007) 265-274.

[14] F. Mirjalili, M. Hasmaliza, L.C. Abdullah, Size-controlled synthesis of nano α-alumina particles through the sol–gel method, Ceramics International 36(4) (2010) 1253-1257.
[15] S. Motaghi, M. Farahmandjou, Structural and optoelectronic properties of Ce–Al_2O_3 nanoparticles prepared by sol-gel precursors, Materials Research Express 6(4) (2019) 045008.
[16] M. Farahmandjou, N. Golabiyan, Synthesis and characterization of Alumina (Al_2O_3) nanoparticles prepared by simple sol-gel method, International Journal of Bio-Inorganic Hybrid Nanomaterials 5(1) (2016) 73-77.
[17] M. Salehi, E. Arabsarhangi, Solution combustion synthesis using Schiff-base aluminum complex without fuel and optical property investigations of alumina nanoparticles, International Nano Letters 5(3) (2015) 141-146.
[18] M. Hakimi, M. Morvaridi, H.A. Hosseini, P. Alimard, Preparation, characterization, and photocatalytic activity of Bi_2O_3–Al_2O_3 nanocomposite, Polyhedron 170 (2019) 523-529.
[19] Z.N. Adamian, H.V. Abovian, V.M. Aroutiounian, Smoke sensor on the base of Bi_2O_3 sesquioxide, Sensors and Actuators B: Chemical 35(1) (1996) 241-243.
[20] L. Leontie, M. Caraman, M. Alexe, C. Harnagea, Structural and optical characteristics of bismuth oxide thin films, Surface Science 507-510 (2002) 480-485.
[21] L. Leontie, M. Caraman, M. Delibaş, G.I. Rusu, Optical properties of bismuth trioxide thin films, Materials Research Bulletin 36(9) (2001) 1629-1637.
[22] V. Fruth, M. Popa, D. Berger, R. Ramer, M. Gartner, A. Ciulei, M. Zaharescu, Deposition and characterisation of bismuth oxide thin films, Journal of the European Ceramic Society 25(12) (2005) 2171-2174.
[23] D. Kulkarni, I.E. Wachs, Isopropanol oxidation by pure metal oxide catalysts: number of active surface sites and turnover frequencies, Applied Catalysis A: General 237(1) (2002) 121-137.
[24] T.-K. Tseng, J. Choi, D.-W. Jung, M. Davidson, P.H. Holloway, Three-Dimensional Self-Assembled Hierarchical Architectures of Gamma-Phase Flowerlike Bismuth Oxide, ACS Applied Materials & Interfaces 2(4) (2010) 943-946.
[25] B. Yang, M. Mo, H. Hu, C. Li, X. Yang, Q. Li, Y. Qian, A Rational Self-Sacrificing Template Route to β-Bi_2O_3 Nanotube Arrays, European Journal of Inorganic Chemistry 2004(9) (2004) 1785-1787.
[26] K. Karthik, K.S. Devi, D. Pinheiro, S. Sugunan, Influence of surfactant on the phase transformation of Bi_2O_3 and its photocatalytic activity, Australian Journal of Chemistry 72(4) (2019) 295-304.
[27] M. Al-Buriahi, F. El-Agawany, C. Sriwunkum, H. Akyıldırım, H. Arslan, B. Tonguc, R. El-Mallawany, Y. Rammah, Influence of Bi_2O_3/PbO on nuclear shielding characteristics of lead-zinc-tellurite glasses, Physica B: Condensed Matter 581 (2020) 411946.
[28] M.K. Trivedi, R.M. Tallapragada, A. Branton, D. Trivedi, G. Nayak, O. Latiyal, S. Jana, Evaluation of atomic, physical, and thermal properties of bismuth oxide powder: An impact of biofield energy treatment, 3(6) (2015) 94-98.
[29] S. Thakur, V. Thakur, A. Kaur, L. Singh, Synthesis and the study of structural, thermal and optical properties of (100-x) Bi_2O_{3-x} (BaO-TiO_2) glass system, Optik 223 (2020) 165646.
[30] B.-H. Yun, Study on Bismuth-based Oxide Ion Conductors with High Performance and Durability for Lower Temperature Solid Oxide Fuel Cells, DGIST, 2020, p. 135.
[31] O.B. Dehkordi, A.M. Hadian, Joining of Alumina to Alumina Using Bismuth Oxide Nano Powder, Procedia Materials Science 11 (2015) 733-737.
[32] K. Kohama, Joining of alumina ceramics using silicon–magnesium composite filler for high-temperature applications, Science and Technology of Welding and Joining 25(5) (2020) 383-390.
[33] F. Cui, Z. Xu, R. Chu, X. He, X. Guo, G. Li, Low temperature sintering ZnO-Bi_2O_3 based varistor ceramics with low electrical breakdown voltage and high nonlinear coefficient, Ceramics International , 47(3) (2020) 4118-4126.
[34] Y. Liao, Y. Wang, Z. Chen, X. Wang, J. Li, R. Guo, C. Liu, G. Gan, G. Wang, Y. Li, Microstructure and enhanced magnetic properties of low-temperature sintered LiZnTiMn ferrite ceramics with Bi_2O_3-Al_2O_3 additive, Ceramics International 46(1) (2020) 487-492.
[35] A.Y. Neiman, A.V. Tanskaya, E.V. Tsipis, L.M. Fyodorova, B.D. Antonov, Effect of size factor on mechanism of interaction between Al_2O_3 and Bi_2O_3 and conductivity of composite on their basis, Nanotechnologies in Russia 6(3-4) (2011) 218-226.
[36] I. Zālīte, L. Grase, S. Lagzdina, D. Rašmane, Porous Ceramics from Al_2O_3 Nanopowders, Key Engineering Materials 850 (2020) 273-278.
[37] S.K. Shubham, R. Purohit, P. Yadav, R. Rana, Study of nano-fillers embedded in polymer matrix composites to enhance its properties–A review, Materials Today: Proceedings 26 (2020) 3024-3029.
D. Yonghao, M. Aiqiong, Z. Dian, G. Yunqin, L. Hongfei, Preparation of high-performance α-Bi_2O_3 photocatalysts and their photocatalytic activity, 8(5) (2020) 295-303.
[39] V. Amendola, I.D. Amans, Y. Ishikawa, N. Koshizaki, S. Scirè, G. Compagnini, S. Reichenberger, I.S. Barcikowski, Room-Temperature Laser Synthesis in Liquid of Oxide, Metal-Oxide Core-Shells, and Doped Oxide Nanoparticles, Chemistry (Weinheim an der Bergstrasse, Germany 26(42) (2020) 9206-9242.
[40] M. Parashar, V.K. Shukla, R. Singh, Metal oxides nanoparticles via sol–gel method: a review on synthesis, characterization and applications, Journal of Materials Science: Materials in Electronics 31 (2020) 3729-3749.
[41] P. Karasiński, A. Domanowska, E. Gondek, A. Sikora, C. Tyszkiewicz, M. Skolik, Homogeneity of sol-gel derived silica-titania waveguide films–Spectroscopic and AFM studies, Optics & Laser Technology 121 (2020) 105840.
[42] H. Ibrahimov, L. Afandiyeva, S. Malikli, G. Rustamli, R. Babali, Obtaining of nanostructured γ-Al_2O_3 by sol-gel method, Thermam (2020) 83.
[43] S. Rahimi, F. SharifianJazi, A. Esmaeilkhanian, M. Moradi, A.H.S. Samghabadi, Effect of SiO_2 content on Y-TZP/Al_2O_3 ceramic-nanocomposite properties as potential dental applications, Ceramics International 46(8) (2020) 10910-10916.
[44] A. Masoudian, M. Karbasi, F. SharifianJazi, A. Saidi, Developing Al_2O_3-TiC in-situ nanocomposite by SHS and analyzingtheeffects of Al content and mechanical activation on microstructure, Journal of Ceramic Processing Research 14(4) (2013) 486-491.
[45] A. Kazemzadeh, M.A. Meshkat, H. Kazemzadeh, M. Moradi, R. Bahrami, R. Pouriamanesh, Preparation of graphene nanolayers through surfactant-assisted pure shear milling method, Journal of Composites and Compounds 1(1) (2019) 25-30.